



Preparation, characterization and electrical behaviors of PEDOT:PSS-Au/Ag nanocomposite thin films: an ecofriendly approach

Ashim Chandra Bhowal¹ · Hrishikesh Talukdar¹ · Sarathi Kundu¹

Received: 11 August 2018 / Revised: 27 November 2018 / Accepted: 7 December 2018 /

Published online: 11 December 2018

© Springer-Verlag GmbH Germany, part of Springer Nature 2018

Abstract

Structure, morphology and electrical behaviors of poly(3,4-ethylenedioxythiophene):poly(4-styrenesulfonate) or PEDOT:PSS thin films are investigated in the presence of protein-mediated green chemically synthesized positively charged gold and silver nanoparticles. The pure and PEDOT:PSS nanocomposite thin films are prepared by spin coating method. The presence of both nanoparticle and polymer is confirmed from X-ray diffraction, whereas composite formation is confirmed from Raman and FTIR spectroscopy. Atomic force microscopy (AFM) images show the surface morphologies of both pure and composite films, whereas average film thicknesses are obtained from AFM and X-ray reflectivity analysis. The presence of electrostatic interaction between the positively charged metallic nanoparticles and negatively charged PSS chains leads to the electrostatic shielding between cationic PEDOT and anionic PSS, which favors better charge transfer through PEDOT–PEDOT conducting paths. The increase in electrical conductivity is visualized from the current–voltage (I – V) curves, which show that the conductivity is relatively higher in the presence of silver than gold nanoparticles in the composite thin films. The conductivity of nanocomposite films is approximately five to six times enhanced in comparison with the pristine PEDOT:PSS thin films.

Keywords PEDOT:PSS-Au/Ag thin films · Nanocomposites · Conductivity · AFM · UV–Vis · FTIR spectroscopy

✉ Sarathi Kundu
sarathi.kundu@gmail.com

¹ Soft Nano Laboratory, Physical Sciences Division, Institute of Advanced Study in Science and Technology, Vigyan Path, Paschim Boragaon, Garchuk, Guwahati, Assam 781035, India

Introduction

Since its discovery in 1978, conducting polymer has become one of the major studied polymeric materials in different fields of science and engineering [1, 2]. It is found that they are very much useful in numerous fields like flexible electronic devices, i.e., electronic circuits mounting on mechanically flexible substrates, organic electrodes, etc. [3]. Among the large numbers of conducting polymers available commercially, some well-studied conducting polymers are poly(aniline), poly(acetylene), poly(phenylenevinylene), poly(vinylpyrrolidone) or PVP, poly(3-hexylthiophene) or P3HT, poly(3,4-ethylenedioxythiophene):poly(4-styrenesulfonate) or PEDOT:PSS, poly(*p*-phenylene sulfide), polyfuran, etc. [4–6]. From the solubility point of view, some conducting polymers are soluble in polar solvents and some are in nonpolar solvents. The polymers those are soluble in water are most popular and largely attractive because of their easy processibility. PEDOT:PSS is easily soluble in water and therefore comparatively easier to work with this polymer. In addition, PEDOT:PSS has some additional benefits like excellent transparency in the optically visible range, better mechanical flexibility, very good thermal performance, low cost, etc. [7–12]. Because of the serious shortage of indium on earth and high cost, PEDOT:PSS may become a relevant candidate instead of ITO, which is generally used for designing optoelectronic devices [8]. However, the electrical conductivity of PEDOT:PSS thin films is quite low and this low conductivity is the major problem for using PEDOT:PSS in different practical applications [13].

The electrical conductivity of PEDOT:PSS thin films can be improved by various treatments. Treatment on PEDOT:PSS films can be made after film preparation by using organic solvents having high boiling points like ethylene glycol, diethylene glycol, 2-nitroethanal, etc. [12, 14, 15] or by using surfactants like dimethyl sulfoxide (DMSO) [16, 17]. Conductivity can also be increased by using organic acid solutions [18], metallic nanoparticles [19–21], cations, anions and zwitterions [2, 22–24], or by using polyelectrolytes [25], etc. PEDOT:PSS is composed of two parts: one is water-insoluble poly(3,4-ethylenedioxythiophene) or PEDOT part and the other is water-soluble polyanionic poly(4-styrenesulfonate) or PSS part. The PSS part is insulating in nature which causes the low conductivity of the pristine PEDOT:PSS. To enhance the conductivity of the PEDOT:PSS films, it is required to reduce the coulombic interaction between the positively charged PEDOT polycations and negatively charged PSS polyanions so that there will a better connectivity between the PEDOT–PEDOT chains and hence the better transfer of electrical charges. There are some reports where after specific treatment/process of the PEDOT:PSS films, some loosely bound or excess PSS chains get rid of the PEDOT:PSS structure to enhance the conductivity of PEDOT:PSS [2, 22, 26]. In the presence of different additives, conformational changes in the PEDOT:PSS structure also take place that enhance the electrical conductivity [25]. The better electrical performances are also obtained through metallic nanoparticles introduction into the PEDOT:PSS matrix using different methods [27–29]. However, more studies are necessary for better understanding of such composite systems for exploring their structural and morphological modifications and the corresponding electrical behaviors.

In this work, we have studied the surface morphology, optical and electrical properties of PEDOT:PSS thin films in the presence of positively charged gold and silver nanoparticles (AuNPs and AgNPs). X-ray diffraction is used to indicate the composite nature of the PEDOT:PSS nanocomposite thin films. Atomic force microscopy (AFM) studies show the surface morphologies of both pure and composite films, whereas average film thicknesses are obtained from AFM and X-ray reflectivity analysis. UV–Vis absorption and steady-state fluorescence are used to identify the modifications in the optical properties of PEDOT:PSS which occur because of the conformational changes of PEDOT and PSS chains. Fourier transform infrared (FTIR) and Raman spectroscopy studies strongly indicate the occurrence of conformational changes in PEDOT:PSS thin films in the molecular level where we found some shifts of vibrational band positions. Electrical measurements are done by using four-probe method which shows nearly five to six times enhancement of conductivity in the presence of AuNPs and AgNPs, i.e., for PEDOT:PSS nanocomposite films. It is also observed that the conductivity is relatively higher in the presence of AgNPs than AuNPs. A mechanism is proposed for improved electrical conductivity of metal nanoparticle-modified polymer films.

Experimental details

Materials

Lysozyme extracted from chicken egg white (Cat. No. 62971, Belgium) was purchased from Sigma-Aldrich and was used as received. Gold (III) chloride trihydrate ($\text{HAuCl}_4 \cdot 3\text{H}_2\text{O}$) (Cat. No. 520918), PEDOT:PSS aqueous solution (Cat. No. 655201, 1.011 g/cm^3 , 3–4% in H_2O) and silver paste (Cat. No. 735825) were purchased from Sigma, and silver nitrate (AgNO_3 , 99% purity) was bought from Merck and was used as received. For optical measurements, films were deposited on quartz substrates and for other measurements deposited on glass substrates having dimension of $2.5 \text{ cm} \times 2.5 \text{ cm}$ by spin coating technique using a spin coater (spinNXG-P2 APEX). Before coating, all substrates were processed with a mixed solution of NH_4OH (30%), H_2O_2 , (30%) and Milli-Q water at a ratio of 2:1:1 (V/V) for 5–10 min at boiling point of water at normal atmospheric pressure. In the next step, all the substrates were properly cleaned with Milli-Q water and dried under air condition.

Preparation of thin films

For the preparation of pristine PEDOT:PSS film on both quartz and glass substrates, $450 \mu\text{L}$ solution of 1.3 wt% was spin coated over substrates at 1000 rpm approximately for 1 min. On the other hand, for the preparation of AuNPs- and AgNPs-treated PEDOT:PSS composite thin films, nanoparticle concentrations were set as 5, 10, 15, 20 and 30 wt%, respectively. For the accurate measurement of nanoparticles concentration, the prepared nanoparticles colloidal solutions were lyophilized to remove water

content and redispersed to get appropriate concentration. Before preparation of the organic–inorganic composite films, each mixed solution containing colloidal nanoparticles and PEDOT:PSS solution was sonicated for short interval of time to get a homogeneous mixture and then the composite solution was spin coated over the different substrates for further characterizations.

Characterization and measurements

UV–Vis spectra were recorded by using Shimadzu spectrophotometer (UV-1800), and the photoluminescence emission spectra were collected from fluorescence spectrometer (Cary eclipse). For the FTIR measurement in ATR-mode, NICOLET 6700 (Thermo Fisher) spectroscopy was used within the wave number range of $4000\text{--}500\text{ cm}^{-1}$ at 4 cm^{-1} resolution. Raman scattering experiments were performed by using *Horiba Jobin Yvon, (Model LabRam), with 514 nm laser source for 10 s duration having scanning power of 20 mW*. Thermal stability of the pristine PEDOT:PSS and composite systems was measured by using thermogravimetric analyzer (PerkinElmer TGA 4000). X-ray diffraction (XRD) and X-ray reflectivity (XRR) measurements were carried out using a D8 Advanced, Bruker, AXS (XRD) setup. The diffractometer consists of a Cu source (sealed tube) followed by a Göbel mirror to select and enhance Cu $K\alpha$ radiation ($\lambda = 1.54\text{ \AA}$). The scattered beam was detected using NaI scintillation (point) detector. XRR data were taken in specular condition; i.e., the incident angle (θ) was kept equal to the reflected angle (θ) such that both lie in the same scattering plane. Under the specular condition, a nonvanishing wave-vector component, q_z , exists which takes the form $(4\pi/\lambda)\sin\theta$. Analysis of XRR data was done using Parratt's formalism [30] where the film is considered as a stack of multiple homogeneous layers having surface and interfacial roughnesses [31, 32]. XRR data effectively provide electron density variation from which out-of-plane structures of the films can be obtained. The surface morphology of the prepared films with and without nanoparticles was well investigated with the help of NTEGRA Prima, NT-MDT Technology, atomic force microscope (AFM) in semi-contact mode with silicon cantilever (spring constant $\approx 11.3\text{ N/m}$). The scanning was done on several portions of each film to get more accurate information. Thicknesses of the pure and composite films were obtained after careful scratching of the thin films using a needle using AFM. The Malvern Zetasizer Nano series, nano ZS90 was used to estimate the average hydrodynamic size and zeta potential value of the prepared AuNPs and AgNPs. The TEM analysis was carried out by using a JEOL JEM-2100 electron microscope. All the conductivity measurements were carried out with the help of Keithley 2635B source meter, and all the electrical connections were done with copper wires. The connections were done at four sides of the PEDOT:PSS films by using silver paste.

Results and discussion

Preparation of silver and gold nanoparticles and their characterization

AuNPs and AgNPs are synthesized using lysozyme protein as lysozyme acts as a reducing cum capping agent. This is a green approach for the synthesis of nanomaterials because various toxic chemicals are not required as reducing and capping agents. Nanoparticles prepared by this particular method have some advantages as such particles are biocompatible in nature and environment friendly. In addition, after nanoparticles formation, proteins cover the nanoparticles, and due to that, nanoparticles possess surface charge which makes them useful for different applications. For particle preparation, the final concentration of lysozyme was 15 mg/mL, whereas the final concentration of gold/silver salt was 1.2 mM. For nanoparticle synthesis, lysozyme solution was taken in a beaker and the salt solution of particular concentration was slowly poured into the protein solution by using a micropipette so that the total volume becomes 20 mL and then the final mixed solution was under constant stirring at ≈ 250 rpm. The color change indicates the completion of the reaction and formation of desired metallic nanoparticles. The time taken for the AuNPs synthesis was ≈ 3 h, and the final color of the solution became moderate pink. However, for AgNPs, the synthesis of nanoparticles took ≈ 2 h and the final color was deep brown. Actually, proteins are very well known for the synthesis of nanoparticles [33–35]. Lysozyme is a small water-soluble globular protein with a molecular weight of $\approx 14,300$ Da and with 129 amino acid residues. The pH of the prepared lysozyme solution was ≈ 5.5 . Isoelectric point of lysozyme protein is ≈ 11.2 , and hence the average surface charge of lysozyme protein molecule was positive at the working pH . The presence of different amino acid residues like tyrosine, tryptophan, lysine, arginine, etc., reduces gold and silver ions and finally forms lysozyme-coated AuNPs and AgNPs [36, 37]. Figure 1a, b shows the UV–Vis spectra of prepared AuNPs and AgNPs. The absorption peaks for gold and silver nanoparticles are observed at ≈ 550 and 390 nm, respectively, which are the characteristic surface plasmon resonance peaks of gold and silver nanoparticles along with a peak at ≈ 273 nm, which is due to the absorption by lysozyme molecules attached on the surface of nanoparticles. Figure 1c, g shows the size distributions of AuNPs and AgNPs, which are found to be $\approx 7.01 \pm 0.80$ nm and 22.06 ± 1.88 nm, respectively. The particle size distributions are shown in Fig. 1e, i. We have calculated the lattice spacing of AuNPs and AgNPs from HRTEM images, which are shown in Fig. 1f, j, respectively. For AuNPs, lattice spacing of 0.19 nm for (200) planes [38] and for AgNPs, lattice spacing of 0.21 nm corresponding to (111) planes are obtained [39].

Figure 2a, b shows the average particle size distribution (hydrodynamic size distribution) of AuNPs and AgNPs obtained from the dynamic light scattering (DLS) technique. The average hydrodynamic size of composite AuNPs and AgNPs is found as ≈ 160 nm and 150 nm, respectively. We have also obtained the zeta potential of prepared nanoparticles (shown in Fig. 2c, d) with the help of zeta analyzer, which is $\approx +25.2$ mV for AuNPs and $\approx +31.4$ mV for AgNPs, respectively.

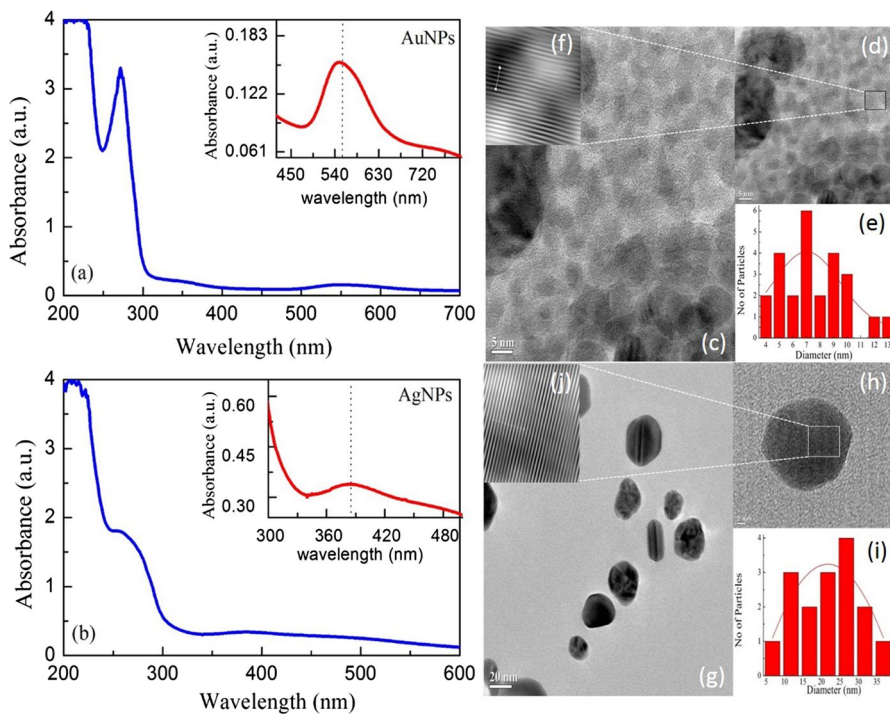


Fig. 1 UV–Vis absorption spectra of lysozyme-coated **a** AuNPs and **b** AgNPs. Insets are the zoomed images of SPR peaks of AuNPs and AgNPs, respectively. **c** TEM image of AuNPs with 5 nm scale bar, **d** zoomed image of AuNPs with 5 nm scale bar, **e** particle size distribution of AuNPs, **f** arrangement of lattice planes of AuNP crystal. **g** TEM image of AgNPs with 20 nm scale bar, **h** HRTEM image of AgNPs with scale bar of 2 nm, **i** particle size distribution of AgNPs and **j** arrangement of lattice planes of AgNP crystal

UV–Vis spectroscopy

UV–Vis absorption spectra of PEDOT:PSS thin films in the presence and absence of AuNPs and AgNPs at three different concentrations, i.e., lower (5 wt%), moderate (15 wt%) and higher (30 wt%) concentrations, are shown in Fig. 3a, b, respectively. From the figures, it is clear that the two peaks are present at ≈ 205 and 278 nm, respectively, and both the peaks are assigned due to the presence of aromatic ring in PSS [40, 41]. The peak present at ≈ 205 nm is due to the bonding to antibonding, i.e., $\pi-\pi^*$, transition, whereas the peak at ≈ 278 nm is due to the bonding to nonbonding, i.e., $\pi-n$, transition of the aromatic rings [42–44]. From the figure, it is clear that the absorptions of the PSS peaks are higher at the lowest concentration of the nanoparticles; however, the absorption decreases with the increasing nanoparticle concentration. Probably the effective number of aromatic rings of PSS chains toward UV–Vis exposure is reduced as the AuNPs/AgNPs concentration is increased, and as a result, the optical absorption value gradually decreases with the increasing particle concentration.

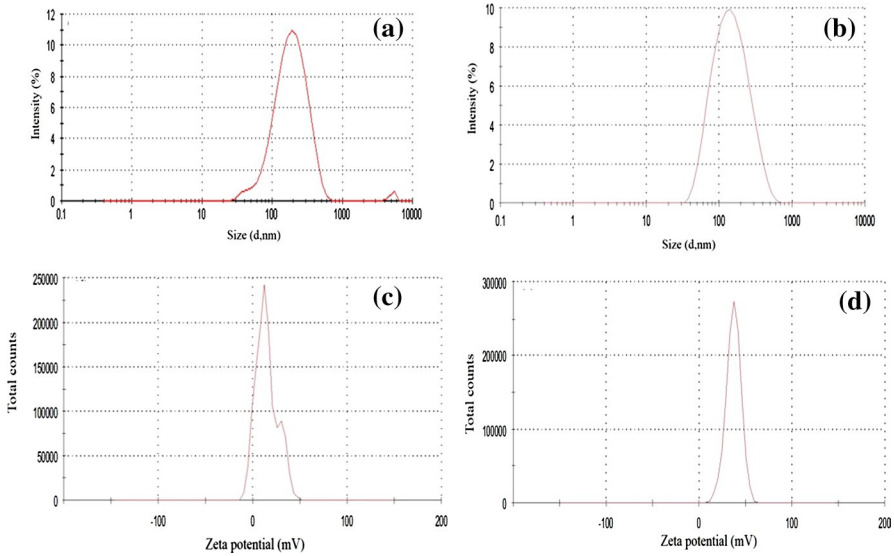
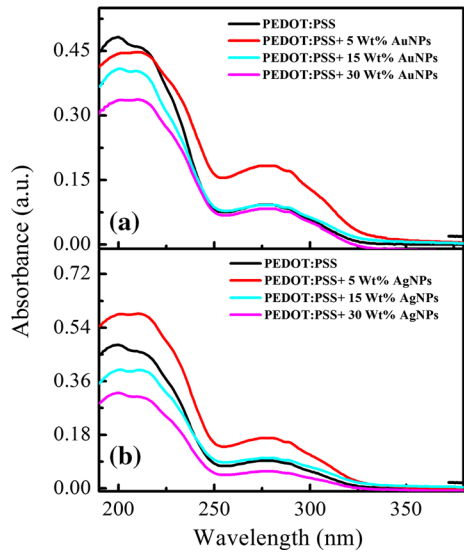


Fig. 2 Average hydrodynamic size distributions of **a** AuNPs and **b** AgNPs. Zeta potential curves for **c** AuNPs and **d** AgNPs

Fig. 3 UV–Vis absorption spectra of **a** pristine PEDOT:PSS films and PEDOT:PSS composite films in the presence of 5, 15 and 30 wt% of AuNPs, respectively, and **b** pristine PEDOT:PSS film and PEDOT:PSS composite films in the presence of 5, 15 and 30 wt% AgNPs, respectively



Photoluminescence spectroscopy

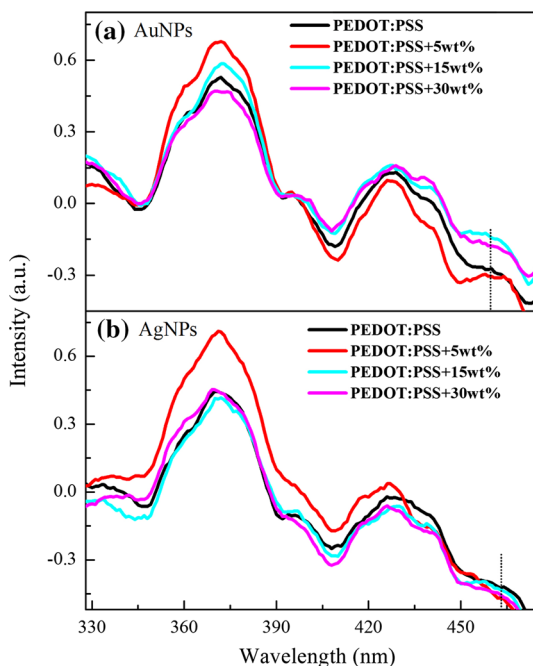
PEDOT:PSS can be used as transparent electrode, and to serve this purpose, it is very important to understand its optical responses in the visible region [45]. We have investigated the photoluminescence property of PEDOT:PSS with and without AuNPs and AgNPs at different concentrations. Fluorescence emission spectra of

PEDOT:PSS are shown in Fig. 4a, b in the presence of AuNPs and AgNPs, respectively, against the excitation wavelength of 278 nm. For both the nanoparticles, emission peaks are observed at ≈ 372 and 430 nm, which is due to the emission from PSS chains [46]. The emission behavior is mostly independent of the nanoparticle concentrations; however, slight intensity variation is there. In addition, there is a signature of weak shoulder emission peak at ≈ 460 nm (marked as dotted line) which is also probably from the PSS chains in the presence of PEDOT/nanoparticles. Our results thus imply that the basic feature of emission is nearly the same for both the pristine and composite films and is nearly independent of the types of nanoparticles and their concentrations; however, slight intensity variation in emissions exists depending upon the nanoparticle concentrations.

Atomic force microscopy

AFM is a very much useful technique to investigate the surface morphology of thin films [16]. Surface morphology and the corresponding phase images of the prepared polymer nanocomposite thin films in the presence of AuNPs and AgNPs are shown in Figs. 5 and 6, respectively. Surface morphology and the corresponding phase images from the pristine PEDOT:PSS film are also exposed for comparison. The average surface roughness obtained from the pristine PEDOT:PSS thin film is ≈ 3.4 nm; however, after mixed with the nanoparticles, little modification is observed on the surface roughness of the films, and the roughness varies from 2.3 to 4.5 nm for the composite films. It is observed from both the topographic and

Fig. 4 Fluorescence emission spectra of pristine PEDOT:PSS thin films and PEDOT:PSS composite films in the presence of **a** AuNPs and **b** AgNPs at lower (5 wt%), moderate (15 wt%) and higher (30 wt%) concentrations of nanoparticles, respectively. Dotted lines indicate shoulder peak at 460 nm



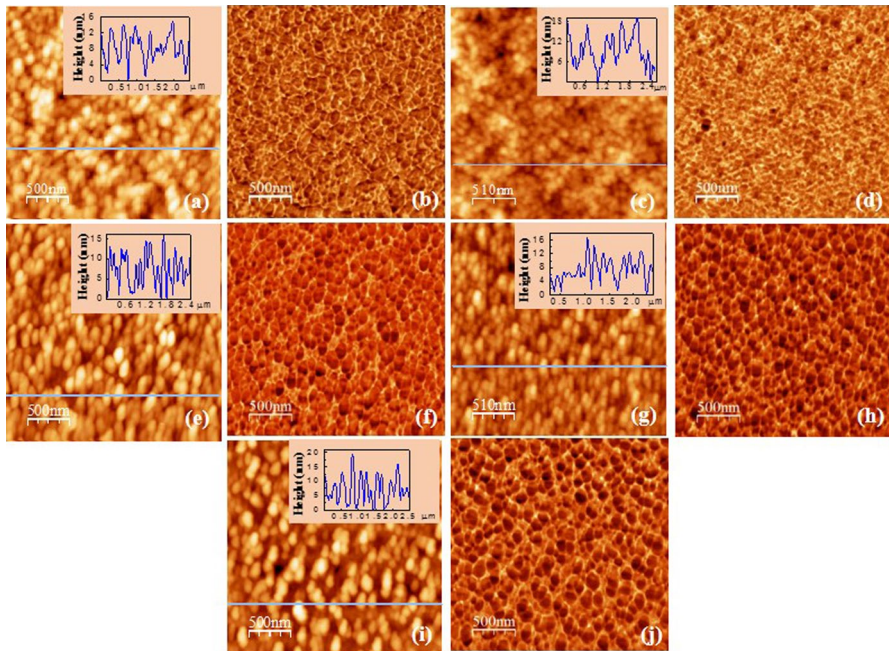


Fig. 5 Surface morphology (**a, c, e, g, i**) and phase (**b, d, f, h, j**) images of pristine PEDOT:PSS and nanocomposite films. **a, b** Pristine PEDOT:PSS. PEDOT:PSS in the presence of AuNPs of **c, d** 5 wt%, **e, f** 10 wt%, **g, h** 15 wt% and **i, j** 20 wt%

phase images that with AuNPs and AgNPs, globule-like or agglomerated structures formed on the surface of the polymer thin films, although such globule-like structure is observed from pristine polymer film also. Highest amount of agglomerated structures are noticed for the 30 wt% of AuNPs and AgNPs, which are observed from both the morphology and phase images. Nanoparticles embedded in the PEDOT:PSS thin films are visible from the phase images, as the dark and bright portions in the phase images are generally responsible for the presence of two different kinds of materials having different mechanical properties, like hardness, viscoelasticity, etc. [47, 48]. The presence of dark and bright portions in the phase images, which are shown in Figs. 5 and 6, clearly signifies the existence of both nanoparticles and PEDOT:PSS in the films, which is much more prominent at the higher nanoparticle concentration.

AFM is one of the promising techniques for the film thickness measurement from the topographic images [49]. A careful analysis of images has been made after scratching of the films using a needle for the film thickness measurements. Figure 7 shows the topographic images around the scratching region of the films, i.e., for (a) pristine PEDOT:PSS, (b) PEDOT:PSS + 5 wt% AuNPs, (c) PEDOT:PSS + 30 wt% AuNPs, (d) PEDOT:PSS + 5 wt% AgNPs and (e) PEDOT:PSS + 30 wt% AgNPs, respectively. Film thicknesses are measured from the corresponding line profiles, which are shown in Fig. 7f–j, respectively. Actual thickness of each film is obtained after measuring the height little far from the edge portion, which is shown

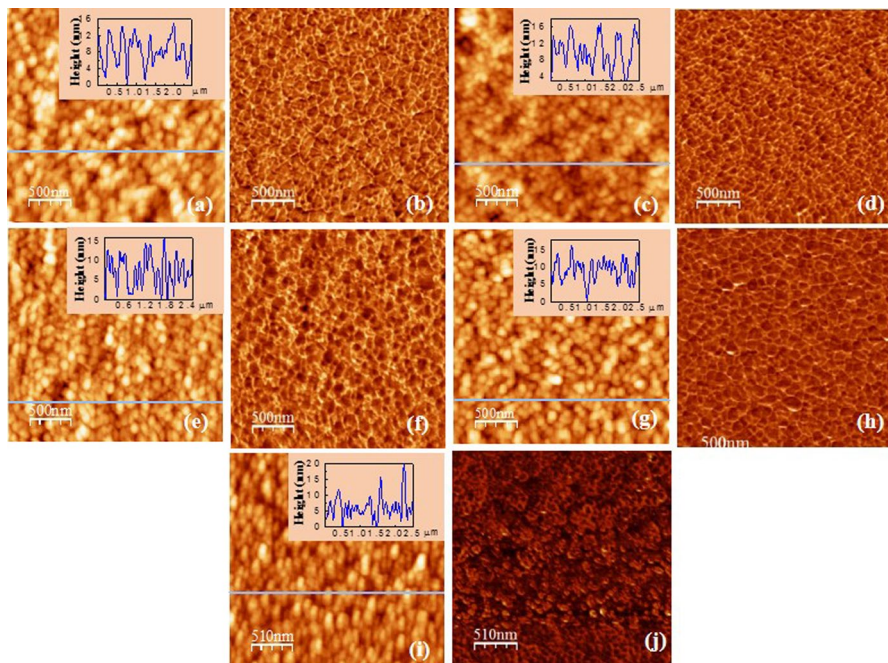


Fig. 6 Surface morphology (**a**, **c**, **e**, **g**, **i**) and phase (**b**, **d**, **f**, **h**, **j**) images of pristine PEDOT:PSS and nanocomposite films. **a**, **b** Pristine PEDOT:PSS. PEDOT:PSS in the presence of AgNPs of **c**, **d** 5 wt%, **e**, **f** 10 wt%, **g**, **h** 15 wt% and **i**, **j** 20 wt%

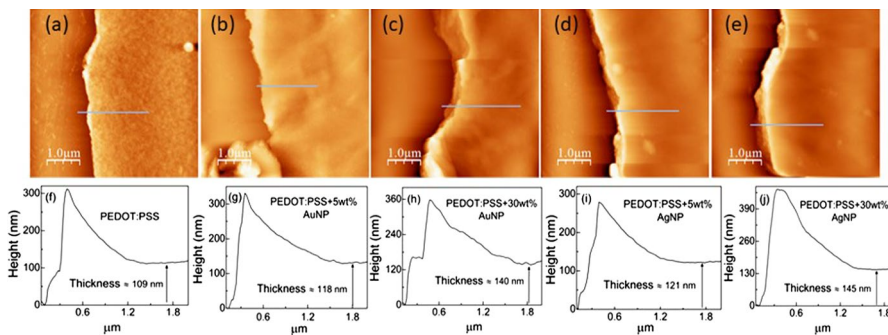


Fig. 7 AFM images for film thickness measurement of **a** pristine PEDOT:PSS, **b**, **c** PEDOT:PSS in the presence of 5 and 30 wt% AuNPs and **d**, **e** PEDOT:PSS in the presence of 5 and 30 wt% AgNPs. **f**, **j** Corresponding line profiles. Vertical arrow indicates the film thickness. Scan area: 5 μm \times 5 μm

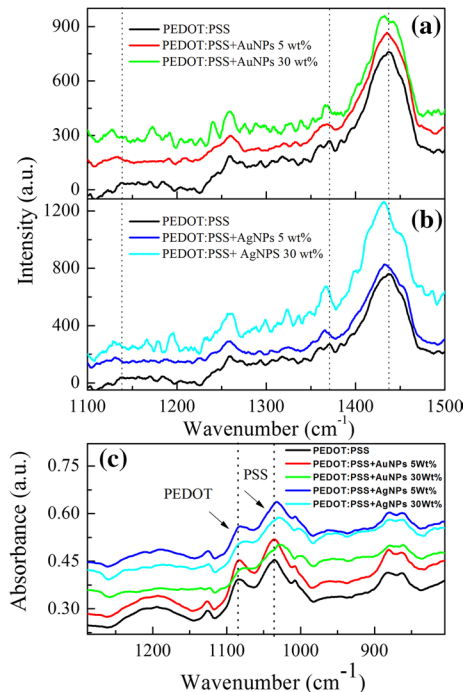
by the straight vertical arrow in each line profile as accumulation of more materials occurs nearly at the edge portion of each scratch as shown in Fig. 7f–j. The pristine PEDOT:PSS thin film shows thickness of ≈ 109 nm, whereas ≈ 118 , 122, 130, 133 and 140 nm thicknesses are obtained from the PEDOT:PSS-AuNPs composite films in the presence of 5, 10, 15, 20 and 30 wt% of AuNPs, respectively. On the other hand, for the PEDOT:PSS-AgNPs composite films, thicknesses of ≈ 121 , 126, 134,

139 and 145 nm are obtained in the presence of 5, 10, 15, 20 and 30 wt% of AgNPs, respectively (all data for film thickness are not shown).

Raman and Fourier transform infrared (FTIR) spectroscopy

Raman spectroscopy is a very useful technique to investigate the conformational changes of polymer and polymer nanocomposites. Conformational changes in the polymer coils affect the vibrational bands of molecules or specific functional groups, which may change the vibrational band positions; i.e., peak shift occurs which gives information about the molecular structure. As shown in Fig. 8a in the case of pristine PEDOT:PSS films, three major bands are identified at $\approx 1137\text{ cm}^{-1}$ (O–S stretching belongs to PSS), 1370 cm^{-1} (C_{β} – C_{β} , inter-ring bonds in PEDOT) and 1440 cm^{-1} (C_{α} = C_{β} , symmetric stretching vibration of PEDOT) [50–53], respectively, and after the introduction of AuNPs, the band positions are shifted to 1133, 1367 and 1435 cm^{-1} for 5 wt%; however, for 30 wt% AuNPs, the band positions are shifted to 1127, 1365 and 1432 cm^{-1} , respectively. Similarly, Fig. 8b describes the band positions of PEDOT:PSS thin films for 5 wt% of AgNPs at $\approx 1130, 1365.5$ and 1432 cm^{-1} , respectively, and for 30 wt% of AgNPs, the band positions are observed at 1128, 1365 and 1431 cm^{-1} , respectively. The strongest peak found at $\approx 1440\text{ cm}^{-1}$ in Raman spectra is due to the C_{α} = C_{β} symmetric stretching vibration of PEDOT, which is associated with the benzoid structure. After nanoparticle treatment, this major peak (observed at $\approx 1440\text{ cm}^{-1}$) of PEDOT is shifted to 1432 and 1431 cm^{-1}

Fig. 8 Raman spectra of **a** pristine and PEDOT:PSS-AuNPs composite thin films (5 and 30 wt%), **b** pure and PEDOT:PSS-AgNPs composite thin films (5 and 30 wt%) and **c** Fourier transform infrared (FTIR) spectra of pristine PEDOT:PSS, and PEDOT:PSS in the presence of 5 and 30 wt% of AuNPs and AgNPs, respectively. Dotted lines indicate the band positions

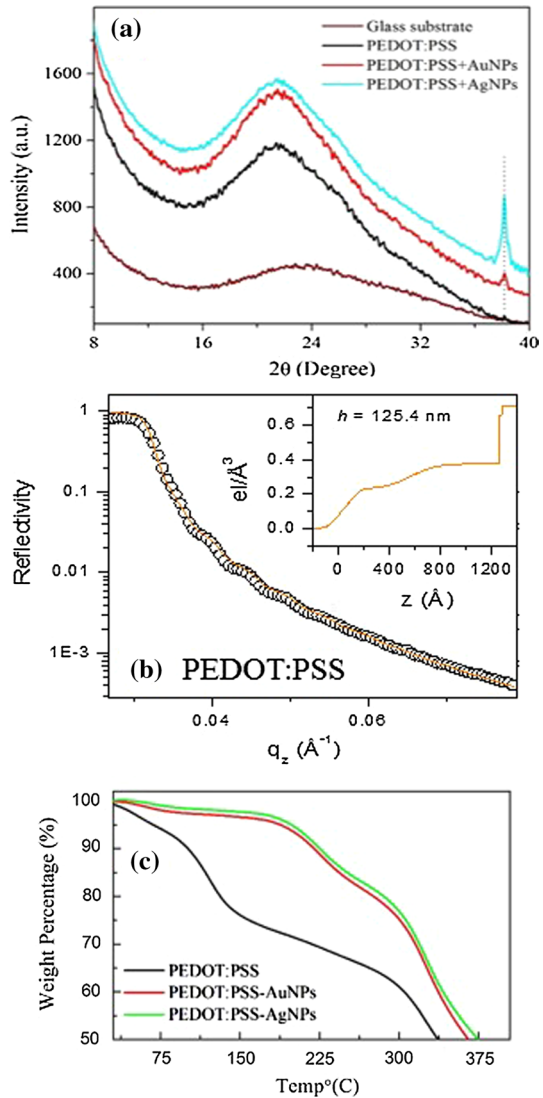


for 30 wt% AuNPs and AgNPs, respectively, which corresponds to the formation of quinoid-like structure. The benzoid and quinoid structures are the coil conformation and the expanded-coil or linear conformation, respectively. Therefore, from the study of Raman spectra, it is identified that conformation of PEDOT changes from benzoid to quinoid structure [54]. The conformational changes of PEDOT:PSS thin films with different concentrations of AuNPs and AgNPs are also well studied by using FTIR spectroscopy and are compared with the pristine PEDOT:PSS. FTIR spectroscopy is a very useful technique to get information in the molecular level; i.e., it can show the changes in the PEDOT:PSS backbone that occurs for the existence of charged nanoparticles in its surroundings. In Fig. 8c, FTIR data are shown for the pristine polymer and polymer in the presence of nanoparticles. In pristine PEDOT:PSS, the vibrational band due to S=O vibration from PSS part is found at 1082 cm^{-1} and after the addition of nanoparticles, the band position is shifted to 1080 cm^{-1} (for 30 wt% AuNPs) and 1079 cm^{-1} (for 30 wt% AgNPs), respectively, whereas for lower concentration of additives (5 wt% AuNPs and AgNPs), vibration of S=O band is obtained nearly at the same position of the pristine polymer. In a similar way, for the pristine PEDOT:PSS film, the initial FTIR band belonging to O–S–O band of PSS is found at 1035 cm^{-1} [55–58] and after the nanoparticles introduction, the band is shifted to 1034 and 1032 cm^{-1} for 5 wt% AuNPs and AgNPs, respectively, and to 1026 and 1028 cm^{-1} for 30 wt% AuNPs and AgNPs, respectively. In addition, PEDOT shows bands at ≈ 1240 and 1070 cm^{-1} due to C–O–C stretching vibrations [55–58] and the peak positions of the bands are slightly shifted in the presence of nanoparticles. Effectively no new FTIR peaks are found but the existing peaks of the pristine PEDOT:PSS are shifted by small amounts due to the presence of both nanoparticles as conformational changes occur in both PEDOT and PSS chains. Thus, in the presence of AuNPs and AgNPs, electrostatic interaction between oppositely charged nanoparticles and PSS takes place and as a result interaction between PEDOT and PSS reduces and conformational modifications occur for both PEDOT and PSS chains. Both Raman and FTIR results confirm the conformational changes of PEDOT and PSS chains in the presence AuNPs and AgNPs and favor the better PEDOT–PEDOT connectivity, which is found through electrical measurements as discussed in the Electrical measurements section.

X-ray scattering and TGA measurements

In Fig. 9a, XRD data are obtained from the glass substrate, pristine PEDOT:PSS and nanoparticles-mixed PEDOT:PSS composite thin films. It is clear from the data that glass substrate shows a broad diffraction peak at $\approx 23.2^\circ$, whereas pristine PEDOT:PSS and PEDOT:PSS in the presence of both AuNPs and AgNPs show a broad peak at $\approx 21.5^\circ$. This implies that very weak crystallinity exists among the polymer chains as the peak is relatively broader and the polymer follows mostly the amorphous nature [59, 60]. The existence of both types of nanoparticles has been confirmed from the presence of sharp peak at $\approx 38.2^\circ$ which is because of the diffraction of X-rays from the (111) plane of gold and silver nanocrystals having fcc structure [61]. Dotted line indicates the XRD peak as obtained from the both AuNPs

Fig. 9 **a** X-ray diffraction data obtained from glass substrate, pristine PEDOT:PSS and PEDOT:PSS nanocomposite thin films in the presence of AuNPs and AgNPs, respectively (bottom to up direction). **b** X-ray reflectivity data (open circle) and the corresponding fitted curve (solid line) from the PEDOT:PSS thin film. Inset: electron density profile, i.e., variation of electron density as a function of height (z). **c** TGA curves of pure PEDOT:PSS, PEDOT:PSS-AuNPs and PEDOT:PSS-AgNPs, respectively



and AgNPs. In Fig. 9b, XRR data collected from the pristine PEDOT:PSS thin film and the corresponding fitted curve show the film thickness. The result obtained from the data fitting shows that the prepared pristine PEDOT:PSS film has thickness of the order of ≈ 125.0 nm, which is obtained from the electron density profile (i.e., in-plane average electron density as a function of depth) as shown in the inset of Fig. 9b. The thickness obtained from the XRR analysis is little higher than the value obtained from the AFM measurement. However, after nanoparticles incorporation, interfacial roughness is enhanced and the XRR data become less informative. Therefore, the thicknesses of the polymer nanocomposite thin films are obtained from the

AFM analysis. The thermal stability of pristine PEDOT:PSS, PEDOT:PSS-AuNPs and PEDOT:PSS-AgNPs composite systems is shown in Fig. 9c. From the thermogravimetric analysis (TGA) curves, it is clear that pristine PEDOT:PSS shows weight loss of 8% at ≈ 70 °C due to water evaporation; however, only slight variation is observed for composite films. Weight loss of $\approx 20\%$ at ≈ 130 °C is seen for pure PEDOT:PSS, whereas in the presence of nanoparticles, similar weight loss occurs at ≈ 250 °C due to the thermal degradation of PSS chains [62]. This indicates that the thermal stability of the PEDOT:PSS is enhanced in the presence of nanoparticles.

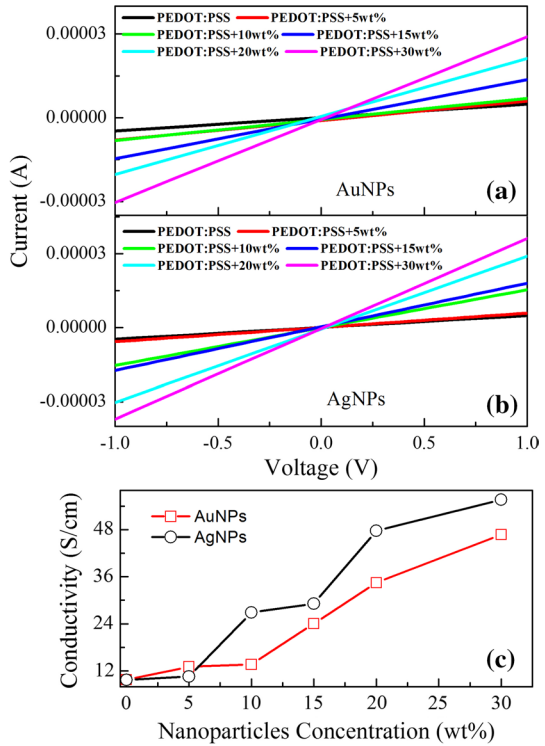
Electrical measurements

For I - V measurements, films are prepared on glass substrates and all the electrical connections are made with the help of thin copper wires. The copper wires are connected on the films at four corners with silver paste. All the connections are carried out according to the four-probe van der Pauw method. The in-plane conductivity of the prepared films is estimated by using the following equation:

$$\sigma = \frac{\ln 2}{\pi d} \left(\frac{I}{V} \right), \quad (1)$$

where σ is the film sample conductivity, d is the film thickness of nearly 125.0 nm, I is the current through the film and V is the voltage across the film sample [63, 64]. In Fig. 10a, b, current–voltage (I - V) responses of PEDOT:PSS films are shown in the presence of AuNPs and AgNPs, respectively. I - V curves clearly indicate that for a particular voltage range, the films conductivity, i.e., flow of current, increases with more and more nanoparticle concentrations. Probably due to the electrostatic interaction between PSS chains and charged nanoparticles, electrostatic screening effect takes place that reduces the interaction between PEDOT and PSS and indirectly helps to have better connection between PEDOT chains and as a result conduction electrons move freely throughout the PEDOT chains which gives better electrical conductivity. For the conductivity measurement, values of the film thicknesses were obtained from the AFM analysis. For the pristine PEDOT:PSS thin film (≈ 109 nm), the conductivity of ≈ 9.76 S/cm is obtained using Eq. (1), and after the inclusion of AuNPs, the conductivity values are become ≈ 13.08 , 13.67, 24.04, 34.46 and 46.73 S/cm for 5, 10, 15, 20 and 30 wt% of AuNPs, respectively. Similarly, in the presence of AgNPs, the conductivity values become ≈ 10.56 , 26.88, 29.14, 47.70 and 55.67 S/cm for 5, 10, 15, 20 and 30 wt% of AgNPs, respectively. Hence, the conductivity values are slightly higher for PEDOT:PSS-AgNPs composite thin films except in the presence of 5 wt% AgNPs, which is shown in Fig. 10c. The conductivity increases nearly five to six times after mixing with the AuNPs and AgNPs, respectively, than the pristine PEDOT:PSS thin film. This relatively higher electrical conductivity in the presence of AgNPs can be understood from the results obtained from the zeta potential measurements. The surface zeta potential value is higher for AgNPs ($\approx +31.4$ mV) in comparison with the AuNPs ($\approx +25.2$ mV), which gives relatively stronger electrostatic interaction between the oppositely charged PSS chains and

Fig. 10 *I*–*V* characteristic curves of **a** pristine PEDOT:PSS and PEDOT:PSS in the presence of 5, 10, 15, 20 and 30 wt% of AuNPs, and **b** pristine PEDOT:PSS and PEDOT:PSS in the presence of 5, 10, 15, 20 and 30 wt% of AgNPs. **c** Comparison of electrical conductivity obtained from PEDOT:PSS nanocomposite films in the presence of AuNPs and AgNPs



AgNPs than the PSS chains and AuNPs and therefore helps to have better electrical connectivity through PEDOT chains.

Mechanism of conductivity enhancement

Our study shows that the conductivity of the PEDOT:PSS thin film is enhanced in the presence of both positively charged AuNPs and AgNPs. The presence of positive charge on the surface of the nanoparticles is confirmed from the zeta potential measurements. Such positively charged nanoparticles attract the negatively charged PSS parts, and due to this electrostatic interaction, PEDOT:PSS chains come closer to nanoparticles, and interconnected conducting paths are generated through PEDOT chains that enhance the electrical conductivity. Enhancement of electrical conducting path through PEDOT chains in the presence of nanoparticles is illustrated in Fig. 11. Moreover, due to the presence of such positively charged nanoparticles, electrostatic screening takes place which weakens the interactions between the PEDOT and PSS chains. As a result, the PEDOT chains become relaxed and take relatively more elongated structural conformation and finally a improved electrical connectivity is achieved between the PEDOT chains in the presence of nanoparticles which enhances the electrical conductivity.

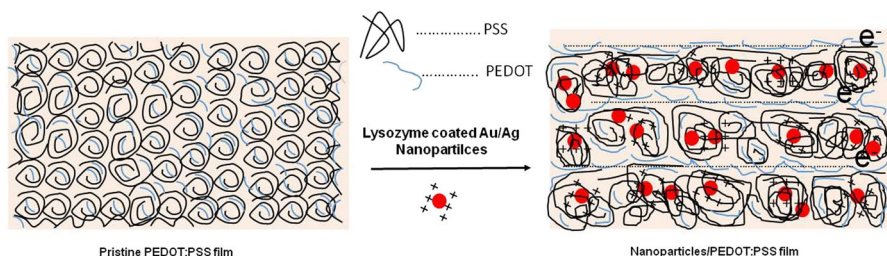


Fig. 11 Schematic illustration of the mechanism of conductivity enhancement of pristine PEDOT:PSS films after incorporation of lysozyme-coated AuNPs and AgNPs. The globule-like morphology of pristine PEDOT:PSS film takes agglomerated structure due to the electrostatic attraction between PSS and positively charged nanoparticles and leads to better connected PEDOT chains and favors better electron movement

Conclusions

The enhancement of electrical behavior of PEDOT:PSS film is established by incorporating positively charged gold and silver nanoparticles. It is found that the presence of positively charged gold and silver nanoparticles modifies the electrostatic interaction between the oppositely charged PEDOT and PSS and a better electrical connectivity is developed between the conducting PEDOT chains which offers a improved conducting path inside the PEDOT:PSS thin films. Raman and FTIR spectroscopy shows such conformational modification of PEDOT and PSS chains after composite formation. Surface morphology, film thickness, composite nature and optical emission of the pristine and composite films are also explored from AFM, XRR, XRD and photoluminescence spectroscopy, respectively. Results obtained from this study clearly confirm that after AuNPs and AgNPs introduction, the electrical response of the composite films is enhanced about approximately five to six times more in comparison with the pristine PEDOT:PSS thin film.

Acknowledgements This study is financially supported by DST, Government of India. Authors would like to acknowledge Dr. Kaushik Das and Mr. Subhankar Pandit for their support during AFM measurements. We would also like to acknowledge CIF, IIT Guwahati, and SAIF, NEHU Shillong, for providing Raman and TEM facility, respectively.

References

1. Skotheim TA, Dekker M (eds) (1986) Handbook of conducting polymers. Marcel Dekker, New York
2. Ouyang J (2013) Secondary doping methods to significantly enhance the conductivity of PEDOT:PSS for its application as transparent electrode of optoelectronic devices. *Display* 34:423–436. <https://doi.org/10.1007/s00289-014-1255-6>
3. Xia Y, Ouyang J (2009) Salt induced charge screening and significant conductivity enhancement of conducting poly (3,4-ethylenedioxythiophene):Poly (styrenesulfonate). *Macromolecules* 42:4141–4147. <https://doi.org/10.1021/ma900327d>

4. Das TK, Prusty S (2012) Review on conducting polymers and their applications. *Polym Plast Technol Eng* 51:1487–1500. <https://doi.org/10.1080/03602559.2012.710697>
5. Nardes AM, Kemerink M, de Kok MM, Vinken E, Maturova K, Janssen RAJ (2008) Conductivity, work function, and environmental stability of PEDOT:PSS thin films treated with sorbitol. *Org Electron* 9:727–734. <https://doi.org/10.1016/j.orgel.2008.05.006>
6. Wynne KJ, Street B (1982) Conducting polymer: a short review. *Ind Eng Chem Prod Res Dev* 21:23–28. <https://doi.org/10.1021/i300005a005>
7. Groenendaal LB, Jonas F, Freitag D, Pielartzik H, Reynolds JR (2000) Poly(3,4-ethylenedioxythiophene) and its derivatives: past, present, and future. *Adv Mater* 12:481–494. [https://doi.org/10.1002/\(SICI\)1521-4095\(200004\)12:73.3.CO;2-3](https://doi.org/10.1002/(SICI)1521-4095(200004)12:73.3.CO;2-3)
8. Xia Y, Ouyang J (2012) Significant different conductivities of the two grades of Poly(3,4-ethylenedioxythiophene):poly(styrenesulfonate), clevios P and clevios PH1000, arising from different molecular weights. *ACS Appl Mater Interfaces* 4:4131–4140. <https://doi.org/10.1021/am300881m>
9. Heywang G, Jonas F (1992) Poly(alkylenedioxythiophene)s-new, very stable conducting polymer. *Adv Mater* 4:116–118. <https://doi.org/10.1002/adma.19920040213>
10. Kirchmeyer S, Reuter K (2005) Scientific importance, properties and growing applications of poly(3,4-ethylenedioxythiophene). *J Mater Chem* 15:2077–2088. <https://doi.org/10.1039/B417803N>
11. Chen Y, Xu J, Yang Y, Zhao Y, Yang W, Mao X, He X, Li S (2016) The preparation and electrochemical properties of PEDOT:PSS/MnO₂/PEDOT ternary film and its application in flexible micro-supercapacitor. *Electrochim Acta* 193:199–205. <https://doi.org/10.1016/j.electacta.2016.02.021>
12. Rivnay J, Inal S, Collins BA, Sessolo M, Stavrinido E, Strakosas X, Tassone C, Delongchamp DM, Malliaras GG (2016) Structural control of mixed ionic and electronic transport in conducting polymers. *Nat Commun* 7:11287–11296. <https://doi.org/10.1038/ncomms11287>
13. Inganas O (2011) Organic photovoltaics: avoiding indium. *Nat Photon* 5:201–202. <https://doi.org/10.1038/nphoton.2011.46>
14. Ouyanga J, Xua Q, Chua CW, Yanga Y, Lib G, Shinarb J (2004) On the mechanism of conductivity enhancement in poly(3,4-ethylenedioxythiophene):poly(styrene sulfonate) film through solvent treatment. *Polymer* 45:8443–8450. <https://doi.org/10.1016/j.polymer.2004.10.001>
15. Wang W, Ruderer MA, Metwalli E, Guo S, Herzig EM, Perlich J, Buschbaum PM (2015) Effect of methanol addition on the resistivity and morphology of PEDOT:PSS layers on top of carbon nanotubes for use as flexible electrodes. *ACS Appl Mater Interfaces* 7:8789–8797. <https://doi.org/10.1021/acsami.5b01327>
16. Yi C, Wilhite A, Zhang L, Hu R, Chuang SSC, Zheng J, Gong X (2015) Enhance thermoelectric properties of Poly(3,4-ethylenedioxythiophene):poly(styrenesulfonate) by binary secondary dopants. *ACS Appl Mater Interfaces* 7(17):8984–8989. <https://doi.org/10.1021/acsami.5b01960>
17. Fan B, Mei X, Ouyang J (2008) Significant conductivity enhancement of conductive Poly(3,4-ethylenedioxythiophene):Poly(styrenesulfonate) films by adding anionic surfactants into polymer solution. *Macromolecules* 41:5971–5973. <https://doi.org/10.1021/ma801245v>
18. Ouyang J (2013) Solution-processed PEDOT:PSS films with conductivities as indium tin oxide through a treatment with mild and weak organic acids. *ACS Appl Mater Interfaces* 5:13082–13088. <https://doi.org/10.1021/am404113n>
19. Breimer MA, Yevgeny G, Sy S, Sadik OA (2001) Incorporation of metal nanoparticle in photopolymerized organic conducting polymers: a mechanistic insight. *Nano Lett* 1:305–308. <https://doi.org/10.1021/nl015528w>
20. Cao Z, Chen Z, Escoubas L (2014) Optical, structural and electrical properties of PEDOT:PSS thin films doped with silver nanoprisms. *Opt Mater Express* 4:2525–2534. <https://doi.org/10.1364/OME.4.002525>
21. Semaltianos NG, Perrie W, Romani S, Potter RJ, Dearden G, Watkins KG (2012) Polymer-nanoparticle composites composed of PEDOT:PSS and nanoparticles of Ag synthesised by laser ablation. *Colloid Polym Sci* 290:213–220. <https://doi.org/10.1007/s00396-011>
22. Yijie X, Ouyang J (2010) Anion effect on salt induced conductivity enhancement of poly(3,4-ethylenedioxythiophene):poly(styrenesulfonate) films. *Org Electron* 11:1129–1135. <https://doi.org/10.1016/j.orgel.2010.04.007>
23. Xia Y, Zhang H, Ouyang J (2010) Highly conductive PEDOT:PSS films prepared through a treatment with zwitterions and their application in polymer photovoltaic cells. *J Mater Chem* 20:9740–9747. <https://doi.org/10.1039/C0JM01593H>
24. Zotti G, Zecchin S, Schiavon G, Louwet F, Groenendaal L, Crispin X, Osikowicz W, Salaneck W, Fahlman M (2003) Electrochemical and XPS studies toward the role of monomeric and

- polymeric sulfonate counterions in the synthesis, composition, and properties of Poly(3,4-ethylenedioxythiophene). *Macromolecules* 36:3337–3344. <https://doi.org/10.1021/ma021715k>
25. Valtakari D, Bollström R, Toivakka M, Saarinen JJ (2015) Influence of anionic and cationic polyelectrolytes on the conductivity and morphology of poly (3,4-ethylenedioxythiophene):poly (styrenesulfonate) films. *Thin Solid Films* 590:170–176. <https://doi.org/10.1016/j.tsf.2006.05.015>
 26. Wang Q, Eslamian M (2016) Improving uniformity and nanostructure of solution-processed thin films using ultrasonic substrate vibration post treatment (SVPT). *Ultrasonics* 67:55–64. <https://doi.org/10.1016/j.ultras.2015.12.012>
 27. Kumar SS, Kumar CS, Mathiyarasu J, Phani KL (2007) Stabilized gold nanoparticles by reduction using 3,4-Ethylenedioxythiophene-polystyrenesulfonate in aqueous solutions: nanocomposite formation, stability, and application in catalysis. *Langmuir* 23:3401–3408. <https://doi.org/10.1021/la063150h>
 28. Xiong Z, Dong C, Cai H, Liu C, Zhang X (2013) Composite inks of poly(3,4-ethylenedioxythiophene)/poly(styrenesulfonate)/silver nanoparticles and electric/optical properties of inkjet-printed thin films. *Mater Chem Phys* 141:416–423. <https://doi.org/10.1016/j.matchemphys.2013.05.035>
 29. Malendez RG, Moreno KJ, Moggio I, Arias E, Ponce A, Llanera I, Moya SE (2010) On the influence of silver nanoparticles size in the electrical conductivity of PEDOT:PSS. *Mater Sci Forum* 644:85–90. <https://doi.org/10.4028/www.scientific.net/MSF.644.85>
 30. Parratt LG (1954) Surface studies of solids by total reflection of X-rays. *Phys Rev* 95:359–369. <https://doi.org/10.1103/PhysRev.95.359>
 31. Daillant J, Gibaud A (1999) X-ray and neutron reflectivity: principles and applications. Springer, Berlin
 32. Tolan M (1999) Reflectivity of X-rays from surfaces. Springer, Berlin
 33. Yang T, Li Z, Wang L, Guo C, Sun Y (2007) Synthesis, characterization, and self assembly of protein lysozyme monolayer-stabilized gold nanoparticles. *Langmuir* 23:10533–10538. <https://doi.org/10.1021/la701649z>
 34. Xie J, Lee JY, Wang DIC (2007) Synthesis of single-crystalline gold nanoparticles in aqueous solution through biomineralization by serum albumin protein. *J Phys Chem C* 111:10226–10232. <https://doi.org/10.1021/jp0719715>
 35. Bakshi MS, Kaur H, Banipal TS, Singh N, Kaur G (2010) Biomineralization of gold nanoparticles by lysozyme and cytochrome c and their application in protein film formation. *Langmuir* 26:13535–13544. <https://doi.org/10.1021/la101701f>
 36. Li L, Liu X, Fu C, Tan L, Liu H (2015) Biosynthesis of fluorescent gold nanoclusters for in vitro and in vivo tumor imaging. *Opt Commun* 355:567–574. <https://doi.org/10.1016/j.optcom.2015.07.023>
 37. Bhargava SK, Booth JM, Agrawal S, Coloe P, Kar G (2005) Gold nanoparticle formation during bromoaurate reduction by amino acids. *Langmuir* 21:5949–5956. <https://doi.org/10.1021/la050283e>
 38. Vallejos S, Stoycheva T, Umek P, Navio C, Snyders R, Bittencourt C, Llobet E, Blackman C, Moniz S, Correig X (2011) Au nanoparticle-functionalised WO₃ nanoneedles and their application in high sensitivity gas sensor devices. *Chem Commun* 47:565–567. <https://doi.org/10.1039/c0cc02398a>
 39. Bindhu MR, Umadevi M (2013) Synthesis of monodispersed silver nanoparticles using Hibiscus cannabinus leaf extract and its antimicrobial activity. *Spectrochim Acta Part A Mol Biomol Spectrosc* 101:184–190. <https://doi.org/10.1016/j.saa.2012.09.031>
 40. Alemu D, Wei HY, Hod KC, Chu CW (2012) Highly conductive PEDOT:PSS electrode by simple film treatment with methanol for ITO-free polymer solar cells. *Energy Environ Sci* 5:9662–9671. <https://doi.org/10.1039/C2EE22595F>
 41. Kim H, Pique A, Horwitz JS, Mattoussi H, Murata H, Kafafi ZH, Chrisey DB (1999) Indium tin oxide thin films for organic light-emitting devices. *Appl Phys Lett* 74:3444–3446. <https://doi.org/10.1063/1.124122>
 42. Xia Y, Sun K, Ouyang J (2012) Highly conductive poly (3,4-ethylenedioxythiophene):poly(styrene sulfonate) films treated with an amphiphilic fluoro compound as the transparent electrode of polymer solar cells. *Energy Environ Sci* 5:5325–5332. <https://doi.org/10.1039/C1EE02475B>
 43. Banwell CN, McCash EM (1995) *Fundamental of molecular spectroscopy*. McGraw-Hill International Limited, UK
 44. Talukdar H, Kundu S (2017) Thin films of protein (BSA, lysozyme)-polyelectrolyte (PSS) complexes show larger red-shift in optical emissions irrespective of protein conformation. *J Mol Struct* 1143:84–90. <https://doi.org/10.1016/j.molstruc.2017.04.074>

45. Koyama T, Matsuno T, Yokoyama Y, Kishida H (2015) Photoluminescence of poly (3,4-ethylenedioxythiophene):poly(styrenesulfonate) in the visible region. *J Mater Chem C* 3:8307–8310. <https://doi.org/10.1039/C5TC01531F>
46. Dimitriev OP, Piryatinski YP, Pud AA (2011) Evidence of the controlled Interaction PEDOT and PSS in the PEDOT:PSS complex via concentration changes of the complex solution. *J Phys Chem B* 115:1357–1362. <https://doi.org/10.1021/jp110545t>
47. Gasiorowski J, Menon R, Hingerl K, Dachev M, Sariciftci NS (2013) Surface morphology, optical properties and conductivity changes of poly(3,4 ethylene dioxy thiophene):poly (styrenesulfonate) by using additives. *Thin Solid Films* 536:211–215. <https://doi.org/10.1016/j.tsf.2013.03.124>
48. Wang X, Kyaw AKK, Yin C, Wang F, Zhu Q, Tang T, Yee PI, Xu J (2018) Enhancement of thermoelectric performance of PEDOT:PSS films by post-treatment with a superacid. *RSC Adv* 8:18334–18340. <https://doi.org/10.1039/c8ra02058b>
49. de Aubin C, Hemmerle SJ, Boulmedais F, Vallat MF, Nardin M, Schaaf P (2012) New 2-in-1 Poly-electrolyte step-by-step film buildup without solution alternation: from PEDOT-PSS to polyelectrolyte complexes. *Langmuir* 28:8681–8691. <https://doi.org/10.1021/la301254a>
50. Barba MS, Kelly AM (2010) Surfaces-enhanced raman study of the interaction of PEDOT:PSS with plasmonically active nanoparticles. *J Phys Chem C* 114:6822–6830. <https://doi.org/10.1021/jp100135x>
51. Wang W, Lei W, Yao T, Xia X, Huang W, Hao Q, Wang X (2013) One-pot of graphene/SnO₂/PEDOT ternary electrode material for supercapacitor. *Electrochim Acta* 108:118–126. <https://doi.org/10.1016/j.electacta.2013.07.012>
52. Zhang L, Peng H, Kilmartin PA, Soeller C, Sejdic JT (2008) Poly(3,4-ethylenedioxythiophene) and polyaniline bilayer nanostructures with high conductivity and electrocatalytic activity. *Macromolecules* 41:7671–7678. <https://doi.org/10.1021/ma8013228>
53. Wang XJ, Wong KY (2006) Effects of a base coating used for electropolymerization of poly (3,4-ethylenedioxythiophene) on indium tin oxide electrode. *Thin Solid Films* 515:1573–1578. <https://doi.org/10.1016/j.tsf.2006.05.015>
54. Sze PW, Lee KW, Huang PC, Chou DW, Kao BS, Huang CJ (2017) The investigation of high quality PEDOT:PSS film by multilayer-processing and acid treatment. *Energies* 10:716–727. <https://doi.org/10.3390/en10050716>
55. Han MG, Foulger SH (2004) Crystalline colloidal arrays composed of Poly(3,4-ethylenedioxythiophene)-coated polystyrene particles with a stop band in the visible regime. *Adv Mater* 16:231–234. <https://doi.org/10.1002/adma.200305642>
56. Kvarnstrom C, Neugebauer H, Blomquist S, Ahonen HJ, Kankare J, Ivaska A (1999) In situ spectroelectrochemical characterization of Poly(3,4-ethylenedioxythiophene). *Electrochim Acta* 44:2739–2750. [https://doi.org/10.1016/S0013-4686\(98\)00405-8](https://doi.org/10.1016/S0013-4686(98)00405-8)
57. Cristovan FH, Nascimento CM, Bell MJV, Laureto E, Duarte JL, Dias IFL, Cruz OW, Marletta A (2006) Synthesis and optical characterization of poly (styrene sulfonate) films doped with Nd(III). *Chem Phys* 326:514–520. <https://doi.org/10.1016/j.chemphys.2006.03.014>
58. Friedel B, Keivanidis PE, Brenner TJK, Abrusci A, McNeill CR, Friend RH, Greenham NC (2009) Effects of layer thickness and annealing of PEDOT:PSS layers in organic photodetectors. *Macromolecules* 42:6741–6747. <https://doi.org/10.1021/ma901182u>
59. Tsujimoto T, Takayama T, Uyama H (2015) Biodegradable shape memory polymeric material from epoxidized soybean oil and polycaprolactone. *Polymer* 7:2165–2174. <https://doi.org/10.3390/polym7101506>
60. Mo Z, Zhang H (1995) The degree of crystallinity in polymers by wide-angle X-Ray diffraction (WAXD). *Rev Macromol Chem Phys* C35(4):555–580. <https://doi.org/10.1080/15321799508021751>
61. Bhowal AC, Kundu S (2016) Time dependent gold nanoclusters and nanocrystals formation on BSA at solid-water and air-solid interfaces. *J Mol Liq* 224:89–94. <https://doi.org/10.1016/j.molliq.2016.09.057>
62. Zhou J, Anjum DH, Chen L, Xu X, Ventura IA, Jiang L, Lubineau G (2014) The temperature-dependent microstructure of PEDOT/PSS films: insights from morphological, mechanical and electrical analyses. *J Mater Chem C* 2:9903–9910. <https://doi.org/10.1039/C4TC01593B>
63. Bahk JH, Favaloro T, Shakouri A (2013) Thin film thermoelectric characterisation techniques, annual review of heat transfer. Begell House Inc., New York
64. Schroder DK (1998) Semiconductor material and device characterization. Wiley, New York